On wake modeling, wind-farm gradients and AEP predictions at the Anholt wind farm

Alfredo Peña[1], Kurt Schaldemose Hansen[1], Søren Ott[1], and Maarten Paul van der Laan[1]

[1]DTU Wind Energy, Technical University of Denmark, Roskilde, Denmark

Correspondence to: Alfredo Peña (aldi@dtu.dk)

Abstract.

We investigate wake effects at the Anholt offshore wind farm in Denmark. We perform the analysis with three commonly-used wake models; two engineering approaches (the Park and G. C. Larsen models) and a linearized Reynolds-averaged Navier-Stokes approach (Fuga). From analysis of SCADA and mesoscale model simulations, we show that for westerly flow in particular, there is a clear horizontal wind-speed gradient over the wind farm, which results from the effect of the land nearby. We also show that for annual energy production estimates, in which a wake model is run with inflow conditions derived from mesoscale model outputs, accounting for the horizontal wind-speed gradient gives nearly the same results as averaging all the wake-free wind climates at the turbines' positions or using the wind climate of a position in the middle of the wind farm. However, annual energy production estimates can largely differ when using wind climates that are strongly influenced by the wind-speed gradient. When looking at westerly flow wake cases, where the impact of the wind-speed gradient is largest, the wake models agree with the SCADA fairly well; when looking at a southerly flow case, where the wake losses are highest, they tend to underestimate the wake loss. With the mesoscale-wake model setup, we are also able to estimate the capacity factor of the wind farm rather well when compared to that derived from the SCADA. Finally, we estimate the uncertainty of the wake models and some of its variants by bootstrapping the SCADA. The models tend to underestimate the wake losses and the engineering wake models are as uncertain as Fuga. These results are specific for this wind farm, the available dataset, and the derived inflow conditions.

1 Introduction

The Anholt wind farm is currently the fourth largest offshore wind farm in the world power-wise. So far the only reported studies on the wake of this wind farm are those of Nygaard (2014), Nygaard et al. (2014), and van der Laan et al. (2017). In the former, there is a comparison between the Park wake model (Katic et al., 1986) and SCADA for a row of turbines in the middle of the wind farm for a given wind-direction and wind-speed range. The wake model does not underestimate the wake losses, which is commonly argued as an issue of the engineering wake models when predicting wakes in large arrays. The study also presents the results of the Park model for different large offshore wind farms, clearly showing that this wake model agrees with the SCADA for different inflow conditions rather well. In the next mentioned study, a comparison of two wake models, Park and the eddy viscosity model of WindFarmer (GL Garrad Hassan, 2013), is performed against SCADA, revealing that Park,

with a wake-decay coefficient $k = 0.04$, gives the best results. In the third study, the effect of the coastline on the wind farm is investigated with a Reynolds-averaged Navier-Stokes (RANS) model, showing that such RANS setup is able to predict the horizontal wind-speed gradient over the wind farm when compared to the SCADA.

Engineering wake models are often regarded as too simplistic for the estimation of wake losses, yet they are those that are

5   most used when planning wind-farm layouts and for annual energy production estimations. This is because they can be easily implemented and optimized in terms of computational performance. One cannot expect to characterize wakes in detail with such models but for the estimation of power and energy production means, they are sufficiently accurate when used properly (Nygaard, 2014; Nygaard et al., 2014). Peña et al. (2014) show that the Park model is able to predict the wake losses of the Horns Rev I wind farm in the North Sea for different atmospheric stability conditions when using a stability-dependent wake-

10   decay coefficient. Peña et al. (2016) show that the Park model is in good agreement with the Sexbierum cases where two more sophisticated wake models are also tested: a linearized RANS solution (Fuga) and a nonlinear solution of the RANS equations that uses a modified k-ε turbulence model. In the latter two studies, the goodness of the results of the Park model is partly a result of accounting for the variability of the wind direction (Gaumond et al., 2014).

The layout of the Anholt wind farm was optimized to minimize wake losses. The number of wind turbines (111), the wind-

15   turbine type and the maximum allowed wind-farm area for turbine deployment (88 km^2) are examples of chosen constraints. The employed optimization tool has a tendency to place most wind turbines at the edges of the wind-farm area, while the remaining wind turbines are placed inside the wind farm with a relative large interspacing. For the particular case of Anholt, a number of wind turbines were relocated from the optimized layout due to seabed that turned to be too soft (Nicolai Nygaard, 2017, personal communication).

20   Wake models of all types have been mainly evaluated against offshore wind farms that are well off the coast or where the effect of the land is assumed to be minimal. The Anholt wind farm can therefore help us investigating such effect as the land is relatively close by and within the direction of the predominant winds. We are aware that the Anholt wind farm experiences strong horizontal wind-speed gradients, which are translated into power gradients for turbines that are not experiencing wakes (Damgaard, 2015). The challenge is therefore to find out how such gradients interfere with the wake losses and how these

25   affect the production and the annual energy production (AEP). To the authors knowledge, there has not been attempts to study the impact of the horizontal wind-speed gradient on wakes of wind farms using engineering wake models yet.

In this study, we first present (Sect. 2) a general background regarding the Anholt wind farm, the mesoscale runs that we use to estimate the wind-farm climate, the wind-farm SCADA, the wake models, and the ways in which we account for the horizontal wind-speed gradient and estimate the wake-models uncertainty. Section 3 presents the results regarding the influence

30   of the wind-speed gradient on flow cases, on the AEP, those showing the evaluation of the wake models for two flow cases, and the analyses of the capacity factor, power loss and model uncertainty. Finally, discussion and conclusions are given in the last two sections.

2   Background

2.1   Definitions

We define the efficiency of the wind farm at a given wind speed U as

$$\eta_U = \frac{\sum_i P_i}{n_t P_U}, \tag{1}$$

where P_i the power of each individual turbine in the farm, P_U the power of the turbine from the power curve at U, and n_t the number of turbines in the wind farm.

We define the power loss of the wind farm as

$$PL = 1 - \frac{\langle \sum_i P_i \rangle}{n_t \langle P_{free} \rangle}, \tag{2}$$

where $\langle \rangle$ means ensemble average and P_{free} is the power of the free-stream turbines (these are defined in Sect. 2.2.2).

We define the relative wake model error as

$$\epsilon = \frac{PL_{obs} - PL_{mod}}{PL_{obs}}, \tag{3}$$

where the subscript $_{obs}$ and $_{mod}$ refer to observations and model, respectively.

2.2   Anholt wind farm

The Anholt wind farm is located in the Kattegat strait between Djursland and the island of Anholt in Denmark (see Fig. 1-left). It consists of 111 Siemens 3.6 MW-120 turbines with hub height of 81.6 m and a rotor diameter of 120 m (Fig. 1-right). The water has depths of 15–19 m, the wind farm area is 88 km^2 and full operation started since summer 2013.

2.2.1   SCADA

We have access to 10-min means of SCADA for the period January 1, 2013 to June 30, 2015. Data include nacelle wind speed, yaw position, pitch angle, rotor speed, power reference, air temperature, rotor inflow speed, and active power. We also produce a filtered SCADA dataset by identifying periods where each turbine was grid connected and produced power during the entire 10-min period. The dataset excludes periods where turbines were either parked or idling, those with starting and stopping events, where power was curtailed, or boosted; power is 5% above rated power for turbines nr. 1, 36, 65, and 68. The result is a time series of 7440 10-min values starting in July 2013 until December 2014.

2.2.2   Inflow conditions

Due to the lack of wake-free mast measurements in the SCADA, we derive the inflow conditions from the filtered SCADA dataset. We estimate an 'equivalent' wind speed from 10-min power and pitch values combined with the manufacturer's power curve. The inflow reference wind speed is estimated as the average equivalent wind speed for wake-free groups of four turbines
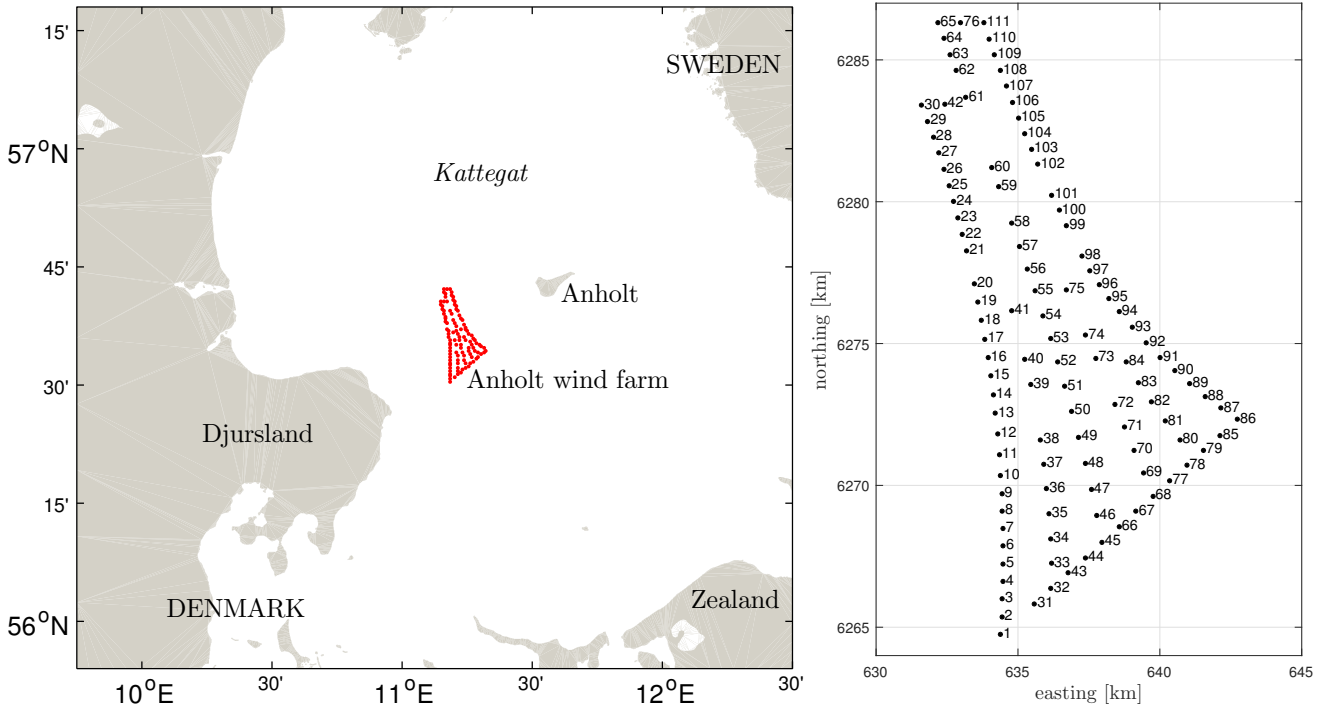
Figure 1. (Left) the Anholt wind farm (red markers) in the Kattegat. (Right) The layout and numbering of the turbines of the Anholt wind farm in UTM32 WGS84

as shown in Table 1. The inflow reference wind direction is estimated as the average of the calibrated, undisturbed wind turbine yaw position of two turbines as shown in Table 2. Due to the large wind farm extension, we also use an additional constraint requiring that nearby wake generating turbines are online during the analysis.

Table 1. Free-stream turbines used to determine the inflow wind speed as function of wind direction

dir [deg]	turbine nr.
0–35	65 76 110 111
35–55	106 107 108 109
55–90	86 87 88 89
90–180	45 66 67 68
180–215	32 43 44 45
215–230	6 7 8 9
230–270	22 23 24 25
270–280	17 18 19 20
280–310	23 24 25 26
310–360	30 65 76 111

Table 2. Free-stream turbines used to determine the inflow wind direction as function of wind direction

dir [deg]	turbine nr.
0–30	65 111
30–90	111 86
90–210	1 86
210–330	1 16
330–360	65 111

2.3   Wind-farm climate

We perform simulations of the wind climate over a region covering the Anholt wind farm using the Weather Research and Forecasting (WRF) version 3.5.1 model. Simulations are carried out on an outer grid with horizontal spacing of 18 km × 18 km (121 × 87 grid points), a first nested domain of 6 km × 6 km (280 × 178 grid points), and a second nest with center in the middle of Jutland, Denmark of 2 km × 2 km (427 × 304 grid points). The simulations use 41 vertical levels from the ground to about 20 km. The lowest 12 levels are within the 1000 m of the surface with the first level at ≈14 m. Initial, boundary conditions, and fields for grid nudging come from the European Centre for Medium Range Forecast ERA-Interim Reanalysis (Dee et al., 2011) at $0.7° × 0.7°$ resolution. Other choices in the model setup are standard and commonly used in the modelling community. Further details regarding the simulations are provided in Peña and Hahmann (2017). Figure 2 shows the Anholt wind climate at hub height at a WRF grid point in the middle of the wind farm based on the WRF hourly outputs for 2014. Most winds come from the west, south-southwest, and southeast directions and winds between 5 and 15 m s^{-1} are the most frequent (the mean wind speed is 9.23 m s^{-1}).
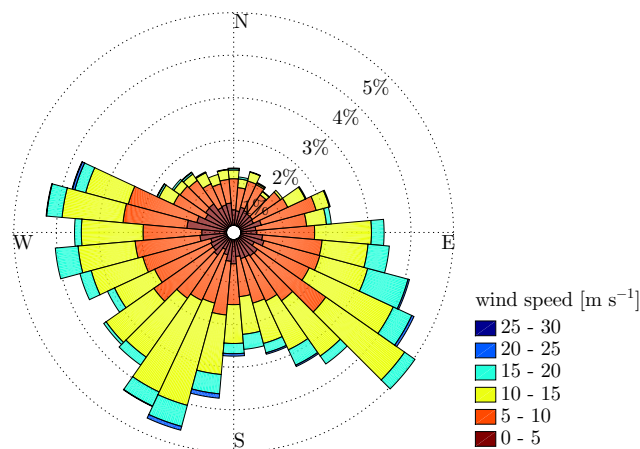
Figure 2. The wind climate at hub height in the middle of the Anholt wind farm for the year 2014 based on WRF simulations

2.4 Wake models

We use three different wake models: the Park wake model with the commonly-used offshore value of $k = 0.04$ with two variants; adding the wake deficits as a quadratic sum (hereafter Park 1) and linearly (hereafter Park 2), the G. C. Larsen model (Larsen, 2009) adding the wake deficits linearly (hereafter Larsen 1) and as a quadratic sum (hereafter Larsen 2), and Fuga

5 (Ott et al., 2011). The first two are engineering wake models and Fuga is a linearized flow solver of the steady-state RANS equations using an actuator-disk approach.

Due to the high computational efficiency of these wake models, we can easily perform wake analysis over given wind-speed and wind-direction ranges and AEP-like calculations in a time series basis. For the latter calculations, we create look-up-tables (LUTs) for each wake model, which contain the total wind-farm power output for specific free wind directions and wind speeds.

10 Figure 3 shows a comparison of the efficiency of the wind farm (Eqn. 1) predicted by the wake models. All wake models show the highest wake losses at the directions where most wind turbines are aligned ($\approx$160/340 and 45/235 deg). At 5 m s^{-1}, the Park 2 model generally shows the highest wake losses followed by Larsen 1 and Fuga (within the direction where turbines are most aligned). At 10 m s^{-1}, $\eta \approx 0.9$ for all wake models excluding the most aligned directions, being Larsen 2 and Park 2 the models showing the highest and lowest efficiencies, respectively; for the Anholt wind climate (Fig. 2) these two models will

15 most probably be the most and less optimistic models, respectively, when performing AEP analysis.
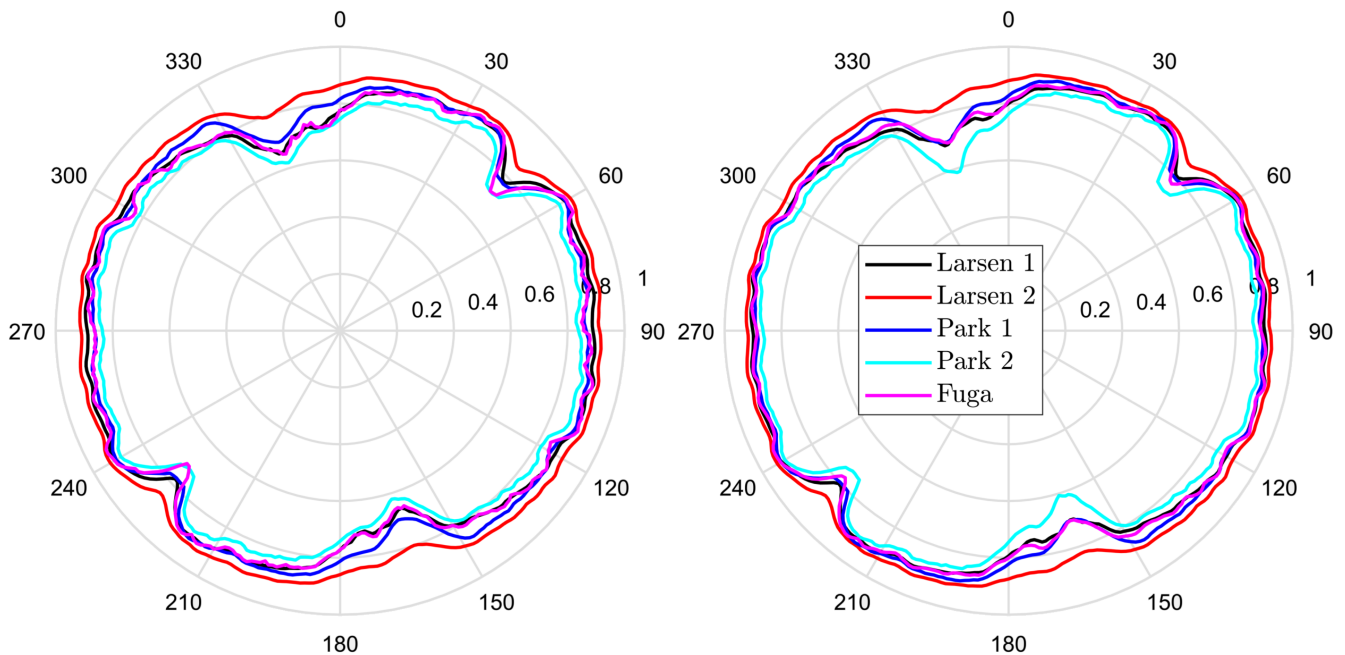
Figure 3. The efficiency of the Anholt wind farm predicted by the wake models at 5 m s^{-1} (left frame) and 10 m s^{-1} (right frame)

2.5 Accounting for the wind-farm gradient

One way to account for the horizontal wind-speed gradient within a wind farm is to estimate the wake losses using the wind speed and direction at each turbine as inflow condition and then average the power estimated at each turbine position (the average is thus computed for the number of turbines in the farm). The wind at each turbine must be wake-free and so mesoscale

5   model simulations over the wind-farm area (without the wind farm) are an obvious option to estimate the wind climate at each turbine position.

Due to the very high efficiency of the Park model (in a Matlab script it takes ≈55 ms to perform one simulation of Anholt for a given inflow wind speed and direction), when using the WRF hourly time series, we can perform 111 simulations (i.e. 111 different inflow conditions that are interpolated from the WRF grid into the turbine positions) in ≈6.1 s. Thus, we can perform

10   a gradient-based AEP analysis with hourly WRF winds in ≈15 h. It is important to note that we can perform AEP calculations with all wake models much faster using the LUTs but these contain the total wind-farm power output only and not the AEP of each individual turbine.

2.6 Uncertainty estimation

We quantify the uncertainty of the wake models using a nonparametric circular-block bootstrap. The idea is to 'wrap' the

15   power-output time series (from both measurements and simulations) of the wind farm around a circle. Blocks of the time series with a given size, which is here selected according to Politis and White (2004) based on the wind-speed time series, are then randomly sampled. The number of sampled blocks is given by the total size of the time series and the block size. The number of bootstrap replications should be large enough to ensure a close to zero Monte Carlo error. By bootstrapping the power-output time series, we can estimate the bootstrapped PL and so estimate a distribution of ϵ. Details and code implementations of a

20   number of bootstrapping techniques can be found at https://www.kevinsheppard.com/images/6/64/AFE_Week_1_handout.pdf.

3 Results

The analysis of the influence of the horizontal wind-speed gradient in Sect. 3.1 is performed with the WRF model outputs for 2014 and the filtered SCADA dataset. For AEP estimations (Sect. 3.1.1), we only use WRF model outputs for 2014. The westerly flow case in Sect. 3.1.2 uses the filtered SCADA dataset, as well as the south flow case in Sect. 3.1.3, and the WRF

25   model outputs for 2014. For the capacity factor calculations in Sect. 3.2, we use all the SCADA available for 2014 and the WRF model outputs for the same year. The analyses of the power loss and model uncertainty in Sects. 3.3 and 3.4 are performed on the filtered SCADA.

3.1 Influence of the wind-farm gradient

Figure 4 shows the mean horizontal wind-speed gradient at hub height in and surrounding the Anholt wind farm based on

30   simulations from the WRF model for the year 2014. The left frame shows the average for all wind speeds and directions

and the right frame the average for all wind speeds and directions within 270 ± 30 deg, which have been filtered using the information at the position of turbine 15. It is clear the influence of Djursland on the wind at the farm even for the all directions case. The impact of Djursland is much stronger when looking at westerly winds so we could expect an impact on the results of wake models when the flow is particulary from these directions. The horizontal wind-speed gradient is mainly due to the

5   roughness effect of the land surrounding the wind farm (van der Laan et al., 2017). Although it is not shown, the island of Anholt east of the farm also has an impact on the wind speed at the wind farm for northeasterly flow but this is not as strong as that of Djursland for westerly flow.
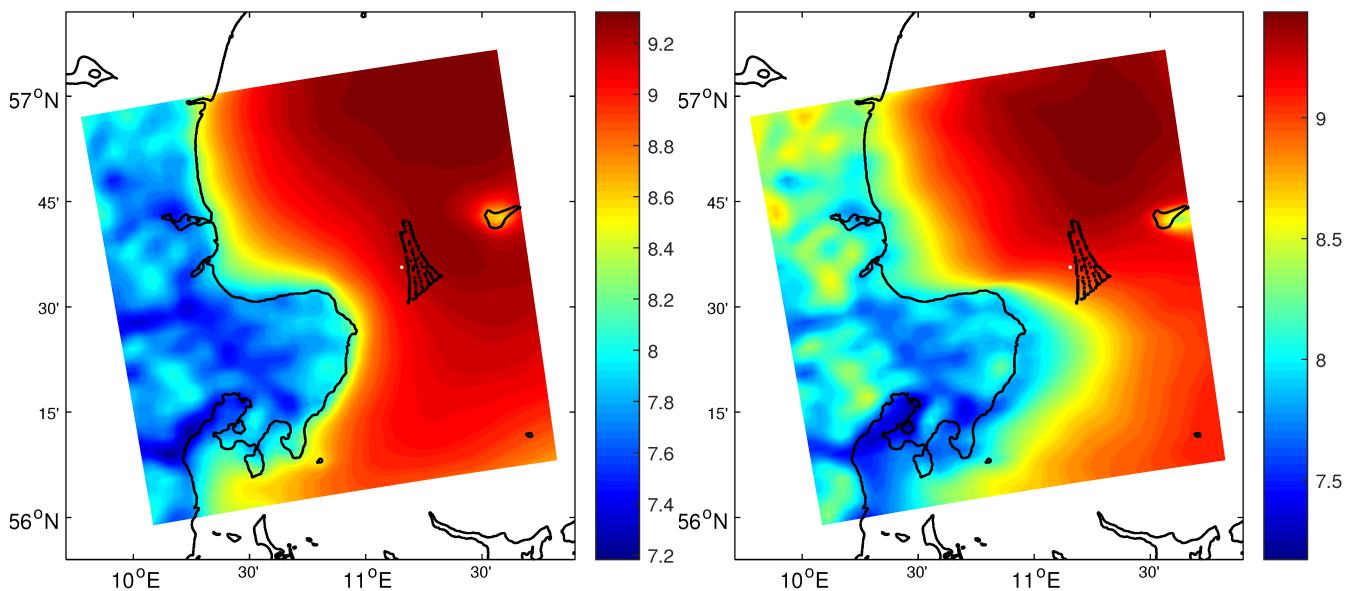
Figure 4. WRF-simulated mean wind speed at hub height on the Anholt wind farm area for the year 2014. All data are shown in the left frame and data within the directions $270 \pm 30°$ at the position of turbine nr. 15 in the right frame. Colorbars are in m s^{-1}

In Fig. 5-left we extract the values from Fig. 4 at each turbine position by linearly interpolating the WRF winds to the turbine positions. For the all directions case, the wind gradient is lower than for westerly winds, as expected, and for both cases the

10   strongest gradient is observed for the first row of turbines (1–30), which are those closer to Djursland.

Figure 5-right shows SCADA-derived and WRF-simulated average wind speeds at hub height for turbines nr. 1–30 for a number of westerly flow cases. We select filtered SCADA based on the inflow conditions described in Sect. 2.2.2 within the wind-speed range 5–10 m s^{-1} and use the manufacturer power curve to derive each turbine's wind speed from the power output. For the comparison, we extract the WRF-simulated winds by averaging the horizontal wind-speed components on the

15   corresponding free-stream turbines for each direction range as given in Table 1. It is observed that the horizontal wind-speed gradient for westerly winds depends on the particular direction. The strongest simulated and observed gradients are found at 265 ± 5 deg, being the winds at turbines nr. 1–15 lower than those at turbines nr. 15–30. Generally, the simulated gradient agrees with the observations fairly well, except for the range 295 ± 5 deg, where the SCADA show the highest winds at the southern

turbines. This might be a effect of the topography on the turbines, which is not captured by WRF, but it is more plausible that this is a wind-farm wall effect (Mitraszewski et al., 2012). A similar effect is observed when analyzing the SCADA-derived wind speeds of the turbines at the south of each row for a direction 80–90 deg: the wind speed at turbine nr. 1 is about 6% higher than that at turbine nr. 86.
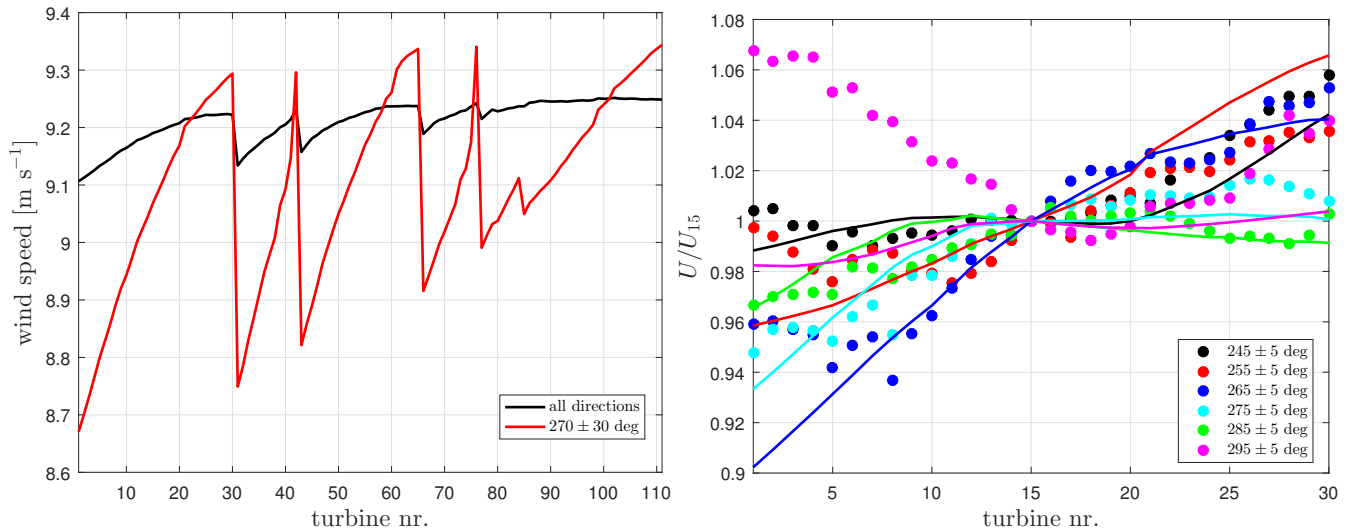
Figure 5. (Left) WRF simulated average wind speed at hub height at the turbine positions of the Anholt wind farm. (Right) Average wind speed at hub height (normalized by that of turbine 15) at the most westerly row of the wind farm for a number of westerly flow cases: WRF winds in solid lines and SCADA-derived winds in markers (details in the main text)

3.1.1 Annual energy production

The difference when accounting for the wind-farm gradient information, as described in Sect. 2.5, to perform the AEP analysis and that that results by assuming a homogenous wind field (estimated each hour by taking the average of the horizontal wind-speed gradient over each turbine of the farm) is not larger than 1% when using the hourly WRF wind fields during 2014 combined with the wake models ('average wind field' column in Table 3). The highest impact is observed for the WRF-Fuga setup, in which the estimation using the 'average wind' does not compensate for the low energy yield of the turbines in the south of the farm and the high energy yield of those in the north as it does for the other WRF-wake model setups.

The difference in the AEP estimation by accounting for the wind-speed gradient and that by using the wind climate of turbine nr. 1, which is the position with the lowest average wind speed, is larger than 1% for the engineering wake models. Such difference is significant considering that the AEP of the wind farm is $\approx$1889.3 GW h when averaging all models' AEP estimations using the wind-gradient information. The same exercise using the information of turbine nr. 54 (in the middle of the farm) results in differences very close to those using the average wind field. Using the information of turbine nr. 65 (at the top of the farm), the difference is also significant but positive as expected. For the Anholt wind farm and its wind climate, in

Table 3. Difference (in percentage) between different type of AEP calculations and that using the horizontal wind-speed gradient information from the WRF simulations

model setup	average wind field	turbine nr. 1	turbine nr. 54	turbine nr. 65
WRF-Park 1	0.05	-1.29	0.08	0.26
WRF-Park 2	0.05	-1.33	0.07	0.26
WRF-Larsen 1	0.05	-1.28	0.08	0.27
WRF-Larsen 2	0.06	-1.24	0.08	0.27
WRF-Fuga	0.76	-0.59	0.77	0.98

particular, these results show that although it is important, accounting for the wind-farm gradient does not change largely AEP estimations compared to those based on a one-point wind climate, unless the latter is not close to the average wind climate within the wind-farm area. For comparison purposes (e.g. with the results in Fig. 5-left) the yearly average wind speed of the 'homogenous' wind is 9.21 m s^{-1}.

3.1.2 Westerly flow cases

So, is the horizontal wind-speed gradient important when studying wake losses under westerly flow conditions? Figure 6-top shows the average[1] WRF-Park 1 power of each turbine in the wind farm when filtering for westerly wind directions (using the simulated wind climate at turbine nr. 15), both accounting for the wind-speed gradient, as described in Sect. 2.5, and assuming a homogenous wind field (the average of the wind climates at each turbine). For a broad wind-direction range, both results are nearly identical and only small differences at specific turbines (up to 27.2 kW) are found when the wind-direction range is reduced; in this latter case we use the range that shows the largest gradients in Fig. 5-right.

Since the horizontal-wind speed gradient does not seem to strongly impact the wake behavior for broad wind-directions ranges, we compare the SCADA that have been wind-speed and direction filtered with the wake models in Fig. 6-bottom. The inflow conditions are derived from the SCADA (see Table 1) and are used to run the wake models. 735 10-min cases are left after filtering for wind speed and direction (5–10 m s^{-1} and 270 ± 30 deg). In this case the normalization is not made with the power of one of the turbines in the west row (1–30), as we did for the plot in the top frame, but with a reference turbine, which is the turbine closest to that where we compute the power from the speed deficit. This aids to levelize the SCADA at turbines nr. 1–30 mainly. The wake models generally agree with the SCADA, particularly Fuga, being this and the engineering wake models' variants using the linear sum of wake deficits those showing the highest wake losses generally. For turbines nr. 31–60, where the wind farm experiences single and double wakes mostly, the SCADA are between the models' results. For turbines nr. 66–111, where multiple wakes occur, Larsen 2 highly underestimates the wake and the linear 'variants' and Fuga seem to generally agree better with the SCADA. However, the comparison is not completely fair with the wake models because the reference power is not always higher or equal to that of the individual turbines when these are supposed to be in the wake of a

---

[1]ensemble average of the 2014 time series
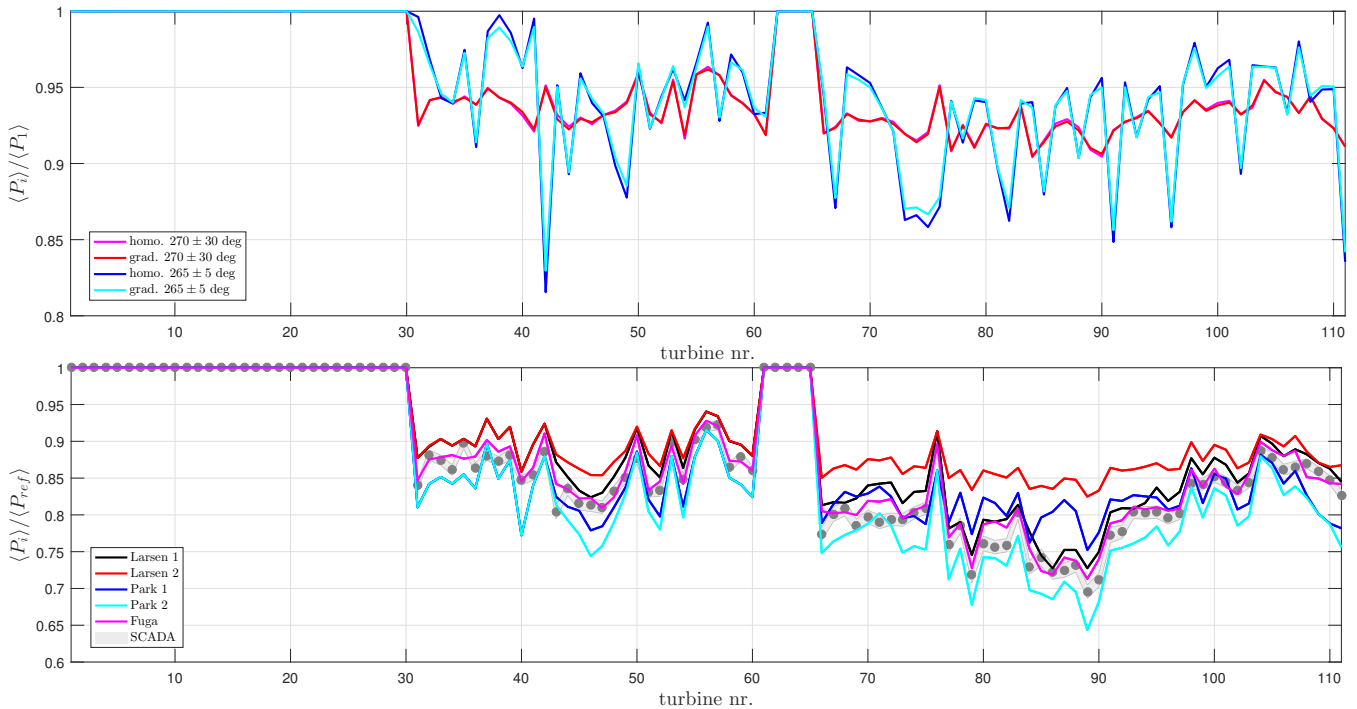
Figure 6. Normalized average power of each turbine in the wind farm for westerly flow conditions. (Top) from simulations using the 2014 WRF time-series and Park 1 with (grad.) and without (homo.) the horizontal wind-speed gradient information. (Bottom) from SCADA and simulations from the wake models within the range 270 ± 30 deg and hub-height inflow wind speed of 5–10 m s^{-1} (details in the main text). For the SCADA, the shaded region indicates $\pm$the standard error

turbine. E.g. in the case of turbine nr. 31, we use turbine nr. 3 as reference and $\approx$19% of the cases with the inflow conditions analyzed in Fig. 6-bottom, $P_3 < P_{31}$.

3.1.3 Southerly flow case

Figure 7 illustrates the wake loss for the north-south row in the middle of the wind farm (turbines nr. 45–65) filtering for inflow

5   conditions (9 ± 0.5 m s^{-1} and 168.7 ± 15 deg) that are derived using the information of the turbines from Table 1. 26 10-min cases are left after filtering for wind speed and direction. As expected from the results in Fig. 6-bottom, for this multiple wake case, the models using the 'linear' variant agree better with the SCADA than those using the 'quadratic' variant when going deeper in the row. The Park 1 model predicts the wake loss of the three first turbines rather well but underpredicts it when moving deeper in the row. The results from Fuga are between the engineering model's variants.

10   Because the differences between SCADA and models in Fig. 7 are relatively large and the amount of 10-min periods for the southerly flow case are 26 only, we also perform actuator-disk RANS simulations in EllipSys3D (Sørensen, 2003) using a modified k-ε turbulence model (van der Laan et al., 2015). The results of the RANS model are very close to those of Fuga
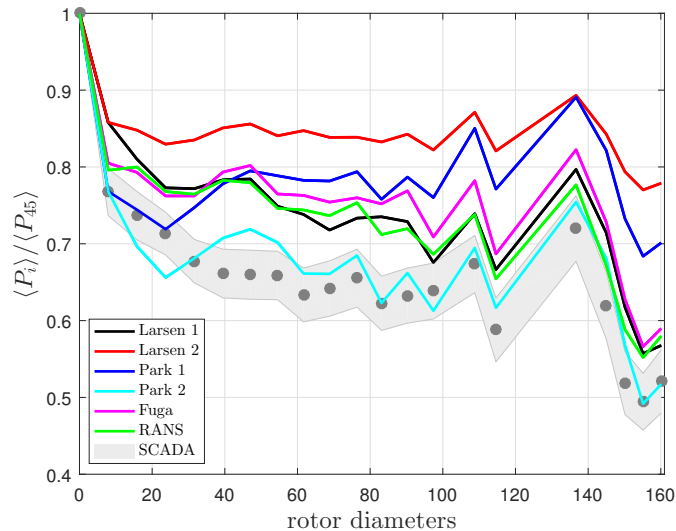
Figure 7. Normalized average power of the north-south row of turbines in the middle of the wind farm for southerly flow conditions from SCADA and simulations from the wake models within the range 168.7 ± 15 deg and hub-height inflow wind speed of 9 ± 0.5 m s^{-1} (details in the main text). For the SCADA, the shaded region indicates $\pm$the standard error

and Larsen 1 also underestimating the wake loss. We can only speculate that for this particular case, the high wake loss from the SCADA is due to atmospheric conditions, in particular a rather stable atmosphere, that we are not accounting for in the simulations. However, we do not have useful observations to directly derive stability. Interestingly, Nygaard (2014) shows the same case using another SCADA period and the wake losses are $\approx$10% lower than those we observe.

3.2 Capacity factor

Being able to estimate the AEP (Sect. 3.1.1) is important but it is more interesting to find out whether we are able to predict it, in our particular case, with the combined mesoscale-wake setup. For the exercise, the capacity factor is a better choice than the AEP, since we can compare Anholt with other offshore wind farms.

We use all the SCADA data that are available for 2014. Theoretically, there should be 52560 10-min samples for this year. However, the amount of samples per turbine available in the SCADA varies and is never the theoretical one; the turbine with the highest samples is nr. 7 (51648) and that with the lowest is nr. 77 (49512). The average availability, taking into account all turbines, of observed samples is 98.10%. Table 4 shows the observed and estimated capacity factors, which are predicted by the WRF-wake model setup and that account for both the wind-farm gradient and the observed average availability of samples.

It is clear that we can estimate fairly well the observed capacity factor using the WRF-wake model setup. However, it is important to note that the turbines are not always working or performing the best so comparing the observed and the predicted AEP/capacity factors is not fair for the combined mesoscale-wake model, although we want to know the capacity factor of a wind farm regardless of the operating conditions.

Table 4. Observed and estimated (from the WRF-wake model setup) capacity factors of the Anholt wind farm for 2014. The estimated values account for the observed average availability of samples

source	capacity factor [%]
SCADA	51.75
WRF-Park 1	53.19
WRF-Park 2	51.89
WRF-Larsen 1	52.87
WRF-Larsen 2	54.13
WRF-Fuga	52.51

3.3 Power loss

Based on the SCADA's 7440 10-min values and using Eqn. (2) with the inflow conditions as defined in Table 1, the wind farm PL is 4.08%. The estimated PL of the wake models are 3.64%, 5.05%, 3.87%, 2.60%, and 3.70% for Park 1, Park 2, Larsen 1, Larsen 2, and Fuga, respectively. The results for the wake models are computed interpolating the models' LUTs with the same inflow conditions derived from the SCADA. All models, except for Park 2, predict lower PLs than the SCADA; Park 1, Larsen 1 and Fuga slightly underestimating the wake loss.

One way to show that the estimations of power of the free-stream turbines are sound is to compare the manufacturer power curve with the SCADA-derived power (averaging the power of the turbines in Table 1) and SCADA-derived inflow wind speed. This is illustrated in Fig. 8-left, where we show the power curve of the turbine and the SCADA-derived free values (no interpolation is made). Figure 8-right shows a similar comparison but in this case we derive the gross wind-farm power (i.e. 111 times the power of the free-stream turbines) and that derived from the power curve at the estimated free wind speed. Both figures show that our definition of the free-stream turbines is sound (no evident wake effects are observed) and that the turbines do follow the manufacturer's power curve.

However, this does not give us an idea about the validity of the SCADA-derived inflow conditions for the turbines that are far from those we use to derive the inflow conditions. Filtering the SCADA-derived inflow conditions for westerly flow (270 ± 30 deg), so that no wakes are observed for turbines nr. 1–30, we can derive power curves for the turbines at the beginning and end of that row (i.e. 1 and 30) and compare them to, e.g. the manufacturer's power curve. As expected, the power curves for turbines nr. 1 and 30 are below and above the manufacturer's one, being the difference as high as 500 kW for turbine nr. 1, which is the turbine with the lowest average wind speed according to the WRF simulations (Fig. 5-left). Within the wind-speed range where we observe such differences in power, the difference in wind speed is about 1 m s^{-1}.

3.4 Model uncertainty

Also based on the SCADA's 7440 10-min values, we found an optimal block length for the circular bootstrap of 242 samples. In average, such sample length corresponds to about 10 days, which is long enough to capture the correlation between samples.
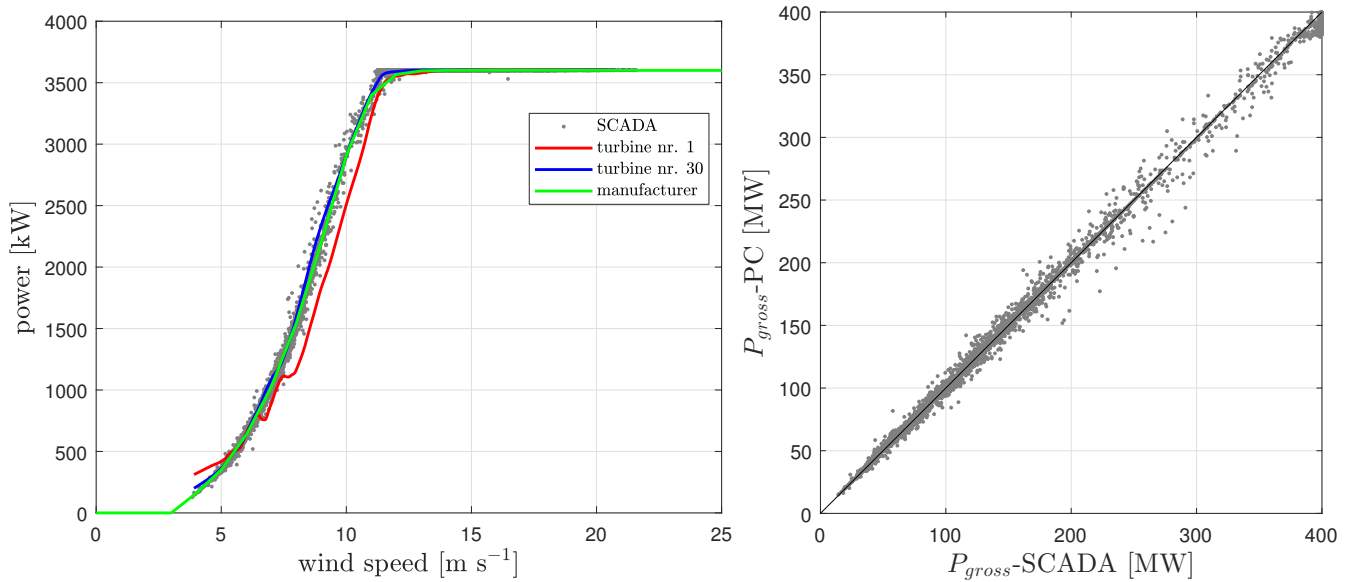
Figure 8. (Left) power curve of the turbines at the Anholt wind farm. (Right) gross wind-farm power derived from the SCADA for the free-stream turbines compared to the that derived from the power curve (PC)

We use 10000 bootstrap replications and found that, e.g. ϵ for the Park 1 model stabilizes after 2000 replications. Figure 9 shows the distribution of ϵ for all models where positive ϵ values denote a model that underestimates the wake loss, whereas negative ϵ values a model that overestimates the wake loss. The mean and standard deviation σ of the distributions of ϵ are given in Table 5.

Table 5. Mean and standard deviation σ of the distribution of the relative error of the wake models

Model	$\langle \epsilon \rangle$ [%]	σ_ϵ [%]
Park 1	10.42	4.84
Park 2	-24.62	7.83
Larsen 1	4.47	5.63
Larsen 2	35.95	3.39
Fuga	8.75	5.17

5   For the particular case of the Anholt wind farm and for the filtered SCADA used in the analysis, Larsen 1 has the distribution with lowest bias and the largest σ values together with Park 2 (both the 'linear' variants), whereas Larsen 2 has the highest bias and lowest σ values. The results for Park 1 and Fuga are very similar, both bias and σ. Park 2, as expected due to the previous results, is the only model systematically overestimating the wake loss. If we could extrapolate these results to an AEP analysis, we would expect non-conservative AEP estimations (except for Park 2), being Park 1, Fuga and Larsen 1 slightly optimistic
10   and Larsen 2 too optimistic.
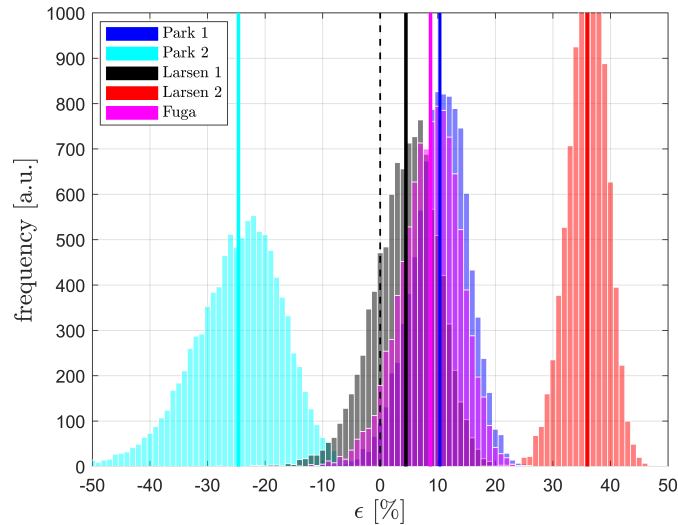
Figure 9. Distribution of the relative model error ϵ (Eqn. 3) of three wake models using 7440 10-min bootstrapped samples from the Anholt wind-farm SCADA. The mean of each distribution is shown with a thicker vertical line

4 Discussion

Some of our results depend on the methods we use to derive the wind-farm inflow conditions. We show that for the individual turbines this is an important matter (see Fig. 8-left), but for this particular wind farm and wind climate, the differences between the inflow derived from turbines in the middle of the long rows and the inflow conditions derived from turbines to either side

5 of the rows seem to compensate for the overall wind-farm long-term analyses (e.g. AEP and capacity factor). One way to further analyze the impact of different inflow conditions is to derive them for each individual wake-free turbine. We can then potentially perform analyses (flow cases, power loss, and capacity factor) in a similar fashion as that we use for accounting for the horizontal wind-speed gradient and validate our findings.

We also estimate the power loss and the uncertainty of the wake models based on a rather discontinuous and short filtered

10 SCADA dataset. Therefore, our results might be biased and caution must be taken when generalizing our findings. A clear example is that related to the model uncertainty where we find that most wake models underestimate the wake losses. With a longer dataset, the biases can change (and models might start to produce conservative results) but the relative position of the modes will most probably be maintained, Park 2 and Larsen 2 being the most conservative and most optimistic models, respectively. This can also happen if the same models are evaluated with SCADA from other wind farms.

15 We show that our WRF-wake model setup is able to predict rather accurately the capacity factor of the Anholt wind farm. Anholt is the offshore wind farm with the highest all-life capacity factor in Denmark (48.7%) and the highest in the world for a wind farm older than 2 y, outperforming Horns Rev II that has in principle more favourable wind conditions. One of the reasons for this is the Anholt wind-farm layout, which highly minimizes the wake losses.

The placement of a wind-turbine row on an arch instead of on a straight line could have a contribution to the minimized wake losses. Wind directions aligned with a straight wind-turbine row typically show well pronounced power deficits for the entire row. When turbines are placed on an arch, the power deficit of the row is less pronounced but smeared out over a larger range of wind directions. In other words, placing wind turbines on an arch has a peak-shaving effect of the power deficit of the

5   wind-turbine row.

5   Conclusions

For the Anholt wind farm, we show from both the SCADA and WRF model simulations that for a number of wind directions, there is a clear influence of the land on the free-stream wind speed at the positions of the turbines closer to the coast. However, for AEP calculations where we run three different wake models using mesoscale model outputs as inflow conditions, accounting

10   for the horizontal wind-speed gradient (also derived from the mesoscale model results) does not have a large impact on the results when compared to AEP calculations based on first, a wind climate that is the average of all wind climates at the turbines' positions, or second, a wind climate correspondent to a position in the middle of the wind farm. It does, however, differ from the calculation using a wind climate that is strongly influenced by the horizontal wind-speed gradient particularly for the engineering wake models.

15   We look at two flow wake cases with two different engineering wake models and some of its variants and a linearized RANS model. The first case corresponds to westerly winds, where the influence of the horizontal wind-speed gradient is largest. Here the wake models, and Fuga in particular, agree with the SCADA fairly well. The second case corresponds to southerly winds, where the wake losses are highest. Here, the wake models tend to underestimate the wake deficit when compared to the SCADA.

20   Using our mesoscale-wake model setup, we find that the estimated capacity factors are 0.27–4.60% biased when compared to that computed from the SCADA. Finally, using inflow conditions derived from the SCADA and by circularly block-bootstrapping these, we estimate the relative error of the wake models. We find that these models tend to underestimate the wake losses, except for one wake model variant. The engineering wake models are found to be as good as the linearized RANS fuga model. However, these are results that are wind-farm and SCADA specific, and that depend on the definition of inflow

25   conditions; therefore similar analyses need to be reproduced at different wind farms, using more SCADA and different methods to derive the inflow conditions.

Data availability. The Anholt SCADA can be made available by DONG Energy upon request to Miriam Marchante Jiménez (mirji@dongenergy.dk). The WRF data can be made available by DTU Wind Energy upon request to Andrea N. Hahmann (ahah@dtu.dk).

Competing interests. The authors declare that they have no conflict of interest.

Acknowledgements. We would like to thank DONG Energy and partners for providing the SCADA. Also, we thank Charlotte B. Hasager to promote and lead the Anholt wind-farm internal project at DTU Wind Energy and Patrick Volker to make the mesoscale model simulation outputs easily accessible.

References

Damgaard, S.: Open issues in wake model validation, http://www.windpower.org/download/2639/08_open_issues_in_wake_model_validationpdf, 2015.

Dee, P. D., Uppala, S. M., Simmons, A. J., Berrisford, P., Poli, P., Kobayashi, S., Andrae, U., Balmaseda, M. A., Balsamo, G., Bauer, P., Bechtold, P., Beljaars, A. C. M., van de Berg, L., Bidlot, J., Bormann, N., Delsol, C., Dragani, R., Fuentes, M., Geer, A. J., Haimberger, L., Healy, S. B., Hersbach, H., Hólm, E. V., Isaksen, L., Kållberg, P., Köhler, M., Matricardi, M., McNally, A. P., Monge-Sanz, B. M., Morcrette, J.-J., Park, B.-K., Peubey, C., de Rosnay, P., Tavolato, C., Thépaut, J.-N., and Vitart, F.: The ERA-Interim reanalysis: configuration and performance of the data assimiliation system, Q. J. R. Meteorol. Soc., 137, 553–597, 2011.

Gaumond, M., Réthoré, P.-E., Ott, S., Peña, A., Bechmann, A., and Hansen, K. S.: Evaluation of the wind direction uncertainty and its impact on wake modelling at the Horns Rev offshore wind farm, Wind Energy, 17, 1169–1178, 2014.

GL Garrad Hassan: WindFarmer v5.2 Theory Manual, Tech. rep., GL Garrad Hassan, 2013.

Katic, I., Højstrup, J., and Jensen, N. O.: A simple model for cluster efficiency, in: Proc. European Wind Energy Assoc. Conf. & Exhibition, Rome, 1986.

Larsen, G. C.: From solitary wakes to wind farm wind fields – a simple enginering approach, Tech. Rep. Risø-R-1727(EN), DTU Wind Energy, 2009.

Mitraszewski, K., Hansen, K., Nygaard, N., and Réthoré, P.-E.: Wall effects in offshore wind farms, http://www.forwind.de/makingtorque/Posters/Poster_77.pdf, 2012.

Nygaard, N. G.: Wakes in very large wind farms and the effect of neighbouring wind farms, J. Phys.: Conf. Ser., 524, 012 162 (10 pp), 2014.

Nygaard, N. G., Clausen, R. S., de Maré, M., and Downey, R.: Benchmarking of wake models for offshore wind farms, in: EWEA Tech. Workshop, Malmö, 2014.

Ott, S., Berg, J., and Nielsen, M.: Linearised CFD models for wakes, Tech. Rep. Risø–R–1772(EN), Risø National Laboratory for Sustainable Energy, 2011.

Peña, A. and Hahmann, A. N.: 30-year mesoscale model simulations for the "Noise from wind turbines and risk of cardiovascular disease" project, Tech. Rep. DTU Wind Energy Report-E-0055(EN), DTU Wind Energy, 2017.

Peña, A., Réthoré, P.-E., and Rathmann, O.: Modeling large offshore wind farms under different atmospheric stability regimes with the Park wake model, Renew. Energ., 70, 164–171, 2014.

Peña, A., Réthoré, P.-E., and der Laan, M. P. V.: On the application of the Jensen wake model using a turbulence-dependent wake decay coefficient: The Sexbierum case, Wind Energy, 19, 763–776, 2016.

Politis, D. N. and White, H.: Automatic block-length selection for the dependent bootstrap, Econometric Rev., 23, 53–70, 2004.

Sørensen, N. N.: General purpose flow solver applied to flow over hills, Tech. Rep. Risø-R-827(EN), Risø National Laboratory, 2003.

van der Laan, M. P., Sørensen, N. N., Réthoré, P.-E., Mann, J., Kelly, M. C., Troldborg, N., Schepers, J. G., and Machefaux, E.: An improved k-ε model applied to a wind turbine wake in atmospheric turbulence, Wind Energy, 18, 889–907, 2015.

van der Laan, M. P., Peña, A., Volker, P., Hansen, K. S., Sørensen, N. N., Ott, S., and Hasager, C. B.: Challenges in simulating coastal effects on an offshore wind farm, J. Phys.: Conf. Ser., 854, 012 046, 2017.